ELSEVIER

Biochimica et Biophysica Acta 1514 (2001) 217–229

BIOCHIMICA ET BIOPHYSICA ACTA
BBA

www.bba-direct.com

# Role of Repeat I in the fast inactivation kinetics of the $Ca_V2.3$ channel

G. Bernatchez, L. Berrou, Z. Benakezouh, J. Ducay, L. Parent *

*Department of Physiology, Membrane Transport Research Group, Université de Montréal, P.O. Box 6128, Downtown Station, Montréal, QC, Canada H3C 3J7*

Received 10 April 2001; received in revised form 14 June 2001; accepted 15 June 2001

**Abstract**

The molecular basis for inactivation in $Ca_V2.3$ (α1E) channels was studied after expression of α1E/α1C ($Ca_V2.3/Ca_V1.2$) chimeras in *Xenopus* oocytes. In the presence of 10 mM $Ba^{2+}$, the CEEE chimera (Repeat I+part of the I–II linker from $Ca_V1.2$) displayed inactivation properties similar to $Ca_V1.2$ despite being more than 90% homologous to $Ca_V2.3$. The transmembrane segments of Repeat I did not appear to be crucial as inactivation of EC(*IS1–6*)EEE was not significantly different than $Ca_V2.3$. In contrast, EC(*AID*)EEE, with the β-subunit binding domain from $Ca_V1.2$, tended to behave like $Ca_V1.2$ in terms of inactivation kinetics and voltage dependence. A detailed kinetic analysis revealed nonetheless that CEEE and EC(*AID*)EEE retained the fast inactivation time constant ($\tau_{fast} \approx 20$–30 ms) that is a distinctive feature of $Ca_V2.3$. Altogether, these data suggest that the region surrounding the AID binding site plays a pivotal albeit not exclusive role in determining the inactivation properties of $Ca_V2.3$. © 2001 Elsevier Science B.V. All rights reserved.

*Keywords:* *Xenopus* oocyte; Structure–function; Site directed mutagenesis; Electrophysiology; Voltage-dependent $Ca^{2+}$ channel; β Subunit

## 1. Introduction

The influx of calcium through voltage-gated $Ca^{2+}$ channels regulates a wide range of cellular processes, including neurotransmitter release, activation of $Ca^{2+}$-dependent enzymes and second messenger cascades, gene regulation, and cell proliferation [1]. Calcium channel inactivation is a critical determinant of the temporal precision of calcium signals and serves to prevent long term increases in intracellular calcium levels. In the L-type $Ca_V1.2$ (α1C) channel, inactivation proceeds mostly in response to a localized elevation of intracellular $Ca^{2+}$ providing negative $Ca^{2+}$ feedback [2,3]. The dominant $Ca^{2+}$ sensor for $Ca^{2+}$-dependent inactivation has recently been identified as calmodulin (CaM), which appears to be constitutively tethered to the channel complex [4–7]. This $Ca^{2+}$ sensor induces channel inactivation by $Ca^{2+}$-dependent CaM binding to an IQ-like motif situated on the carboxyl tail of $Ca_V1.2$ [8].

Voltage-dependent inactivation appears to be the key mechanism by which non-L-type $Ca^{2+}$ channels achieve regulation of internal calcium levels. Unlike the well characterized ball and chain and hinged lid inactivation mechanisms of voltage-dependent potassium [9] and sodium [10,11] channels, the molecular mechanisms for voltage-dependent inactivation in $Ca^{2+}$ channel proteins are incompletely understood. It has been previously reported that Repeat I plays a role in voltage-dependent gating of $Ca^{2+}$ channels

* Corresponding author. Fax: +1-514-343-7146.
*E-mail address:* lucie.parent@umontreal.ca (L. Parent).

0005-2736/01/$ – see front matter © 2001 Elsevier Science B.V. All rights reserved.
PII: S0005-2736(01)00373-X

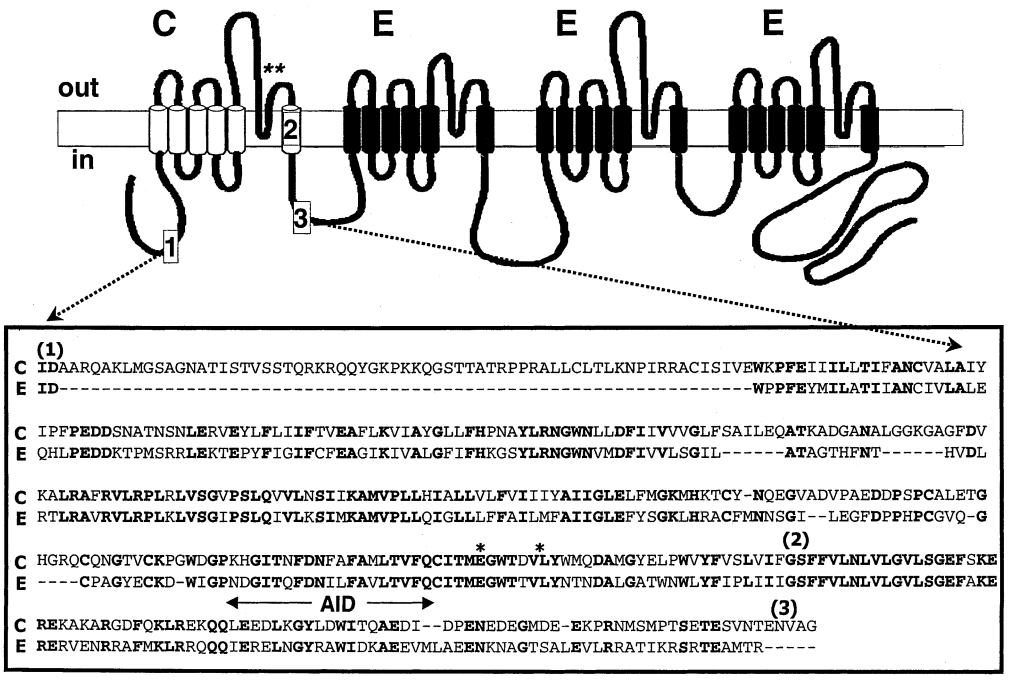


Fig. 1. CEEE was obtained by swapping the 1–3 region between $Ca_V2.3$ and $Ca_V1.2$. Chimera EC(*AID*)EEE was obtained by introducing the 2–3 region of $Ca_V1.2$ into $Ca_V2.3$. CEEE and EC(*AID*)EEE differ from $Ca_V2.3$ by 160 and 50 residues, respectively. Chimera EC(*IS1–6*)EEE was produced using the larger 1–2 region. Identical residues are shown in bold. The pore region is indicated by a double asterisk (**) and the β-subunit binding site is marked (AID).

with effects on both activation [12,13], and inactivation gating [14,15]. Studies with $Ca_V2.3/Ca_V2.1$ chimeras strongly suggested that Repeat I, and more precisely IS6, could confer faster inactivation to $Ca_V2.1$ channels [14]. Repeat II has also been hailed as a key player in that process [16] although this conclusion has somewhat been revised in favor of the I–II linker [17]. We have recently shown that point mutations in the I–II linker of $Ca_V2.3$ channels, and more specifically in the nonconserved residues of the β-subunit binding motif, disrupted specifically the kinetics and voltage dependence of inactivation whereas reverse mutations in $Ca_V1.2$ accelerated inactivation kinetics [18,19]. The R378 position in the middle of the AID motif in the human $Ca_V2.3$ channel was shown to be particularly critical in that process whereas voltage-dependent inactivation appeared to be less sensitive to other point mutations in that region [18]. Nonetheless, no point mutation within the AID motif could completely eliminate voltage-dependent inactivation in $Ca_V2.3$ and revert to the $Ca_V1.2$ inactivation phenotype [18].

In view of these differences, we undertook to study the molecular mechanisms underlying voltage-dependent inactivation in α1E ($Ca_V2.3$) channels using $Ca_V2.3$/ $Ca_V1.2$ chimeras. Our results confirm that part of the I–II linker of $Ca_V1.2$ can confer slower inactivation kinetics and lesser voltage dependence onto $Ca_V2.3$ channels. In particular, the EC(*AID*)EEE chimera, which includes the β-subunit binding domain from $Ca_V1.2$ was faster than CEEE whereas EC(*IS1–6*)EEE was not significantly different than $Ca_V2.3$ [19]. The inclusion of the complete AID motif from $Ca_V1.2$ nonetheless failed to completely convert the inactivation phenotype of $Ca_V2.3$ into $Ca_V1.2$, thus suggesting a key role for other regions of the $Ca_V2.3$ subunit.

## 2. Material and methods

### 2.1. Recombinant DNA techniques

Standard methods of plasmid DNA preparation were used [20]. To obtain the chimeras, a site *Xho*I was first engineered by polymerase chain reaction into α1C (GenBank 15539) at 1530 nt (Fig. 1, position 3). The $Ca_V1.2$ (*Xho*I) or α1C (*Xho*I) channel

was not significantly different than the wild-type $Ca_V1.2$ (Table 1). The chimeras ECCC and CEEE were obtained by swapping Repeat I between the *Cla*I and *Xho*I sites (Fig. 1, positions 1–3). The ECCC chimera never yielded functional calcium channels after expression in *Xenopus* oocytes. Chimera EC(*AID*)EEE was obtained by introducing the *Bam*HI/*Xho*I segment (Fig. 1, positions 2–3) into $Ca_V2.3$. The $Ca_V1.2$ fragment present in this chimera extends from the middle of IS6 to the middle of the I–II linker. Taking into account that the 3′ end of IS6 is strictly conserved between the two channels, this $Ca_V1.2$ fragment is $\approx 50$ amino acids (aa) larger than the AID motif. Nonetheless, for simplicity's sake the resulting chimera is simply referred to as EC(*AID*)EEE throughout the text. The actual CE(*AID*)CCC chimera in which the eight nonconserved residues within the AID motif from $Ca_V1.2$ were mutated into their counterpart in $Ca_V2.3$ (LEDKLDTQ/IRENRADK) failed to express significant whole-cell barium currents. These multiple mutations were introduced directly into the wild-type $Ca_V1.2$ channel using the Quick-Change XL-mutagenesis kit (Stratagene, La Jolla, CA). Chimera EC(*IS1–6*)EEE was obtained by introducing the *Cla*I/*Bam*HI fragment of $Ca_V1.2$ (Fig. 1, positions 1–2) into $Ca_V2.3$. Constructs were verified by restriction mapping and recombinant clones were screened by double-stranded sequence analysis of the entire ligated cassette. The nucleotide sequence of the mutated region was analyzed using automatic sequencing by BioST (Lachine, QC). Run-off transcripts were prepared using methylated cap analog $m^7G(5')ppp(5')G$ and T7 RNA polymerase with the mMessage mMachine® transcription kit (Ambion, Austin, TX).

### 2.2. Functional expression of wild-type and mutants channels

Female *Xenopus laevis* clawed frog (Nasco, Fort Atkinson, WI) were anesthetized by immersion in 0.1% tricaine or MS-222 (3-aminobenzoic acid ethyl ester, Sigma, St. Louis, MO) for 15 min before surgery as detailed before [3,21,22]. Stage V and VI oocytes were injected with cRNA coding for the α1 subunits (chimeras and wild-type) along with cRNA coding for rat brain α2bδ [23], and either rat brain β3 [24], rat brain/cardiac β2a [25], or rat brain β1b [26] using typically a weight ratio of 3:1:1 for α1/α2/β. Oocytes were incubated at 19°C in a Barth's solution for 3–5 days before experiments.

### 2.3. Electrophysiological recordings in oocytes

Whole-cell currents were recorded at room temperature using a two-electrode voltage-clamp amplifier (OC-725C, Warner Instruments) as described earlier [15,18,22]. Unless stated otherwise, currents were measured with a 10 $Ba^{2+}$ solution (in mM: 10 $Ba(OH)_2$; 110 NaOH; 1 KOH; 20 HEPES titrated to pH 7.3 with methane sulfonic acid (MeS)). Currents were occasionally recorded in a 10 CaMeS so-

Table 1
Biophysical properties of α1E ($Ca_V2.3$) and α1C ($Ca_V1.2$) channels and chimeras

| Channels with α2bδ/β3 (10 $Ba^{2+}$) | Inactivation (5 s) | | Peak $I_{Ba}$ (μA) |
|---|---|---|---|
| | $E_{0.5}$ (mV) | $z$ | |
| α1E wt | −64 ± 3 (9) | 3.5 ± 0.4 | −3.7 ± 1.3 (21) |
| EC(*IS1–6*)EEE | −57 ± 2 (4) | 3.5 ± 0.5 | −3.4 ± 2.4 (5) |
| EC(*AID*)EEE | −30 ± 2 (6)*** | 3.2 ± 0.3 | −5.1 ± 1.1 (8) |
| CEEE | −23 ± 1 (5)*** | 3.2 ± 0.4 | −1.7 ± 1.1 (6) |
| ECCC | N.D. | N.D. | No expression |
| α1C (*XhoI*) | −23 ± 3 (8)*** | 3.4 ± 0.4 | −3.3 ± 0.3 (9) |
| α1C wt | −20 ± 4 (12)*** | 3.1 ± 0.4 | −3.9 ± 0.5 (17) |

Biophysical parameters of channels expressed in *Xenopus* oocytes with α2bδ and β3 subunits and recorded in 10 mM $Ba^{2+}$. The voltage dependence of inactivation was determined from isochronal inactivation data (5 s) as shown in Fig. 4. Relative currents were fitted to Boltzmann Eq. 1. Peak $I_{Ba}$ was determined from *I–V* relationships measured for the corresponding experiments. The data are shown as mean ± S.E.M. and the number $n$ of samples appears in parentheses. Student $t$-tests were performed between $Ca_V2.3$ and other channels, with $P < 0.001$ (***).

lution where $Ca(OH)_2$ replaced $Ba(OH)_2$ equimolarly. To minimize endogenous $Ca^{2+}$ activated $Cl^-$ currents, oocytes were injected with 18.4 nl of a 50 mM EGTA (ethyleneglycol bis(β-aminoethylether)-*N*,*N*,*N*′,*N*′-tetraacetic acid) (Sigma) 1–2 h before the experiments.

### 2.4. Data acquisition and analysis

PClamp software (Axon instruments, Foster City, CA) was used for on-line data acquisition and analysis. Data were sampled at 10 kHz and low-pass filtered at 5 kHz using the amplifier built-in filter. The currents were elicited from a holding potential of −80 mV and measured using a series of voltage pulses from −40 to +60 mV. Current traces were corrected for linear leak and cell capacitance. Isochronal inactivation data (pseudo h inf) were measured at the test pulse of 0 mV after a series of 5-s prepulses applied from −100 to +30 mV [15].

$$\frac{i}{i_{max}} = 1 - \frac{1 - Y_0}{1 + \left\{ \exp - \frac{zF}{RT}(V_m - E_{0.5}) \right\}} \quad (1)$$

Pooled data (mean ± S.E.M.) were fitted to the Boltzmann Eq. 1 which accounts for the fraction of non-inactivating current with $E_{0.5}$, mid-point potential; $z$, slope parameter; $Y_0$, fraction of non-inactivating current; $V_m$, the prepulse potential, and $RT/F$ with their usual meanings.

Inactivation time constants were measured at 450 ms. Leak subtracted current traces were fitted to a multi-exponential equation using a built-in function in Clampfit 6.2.

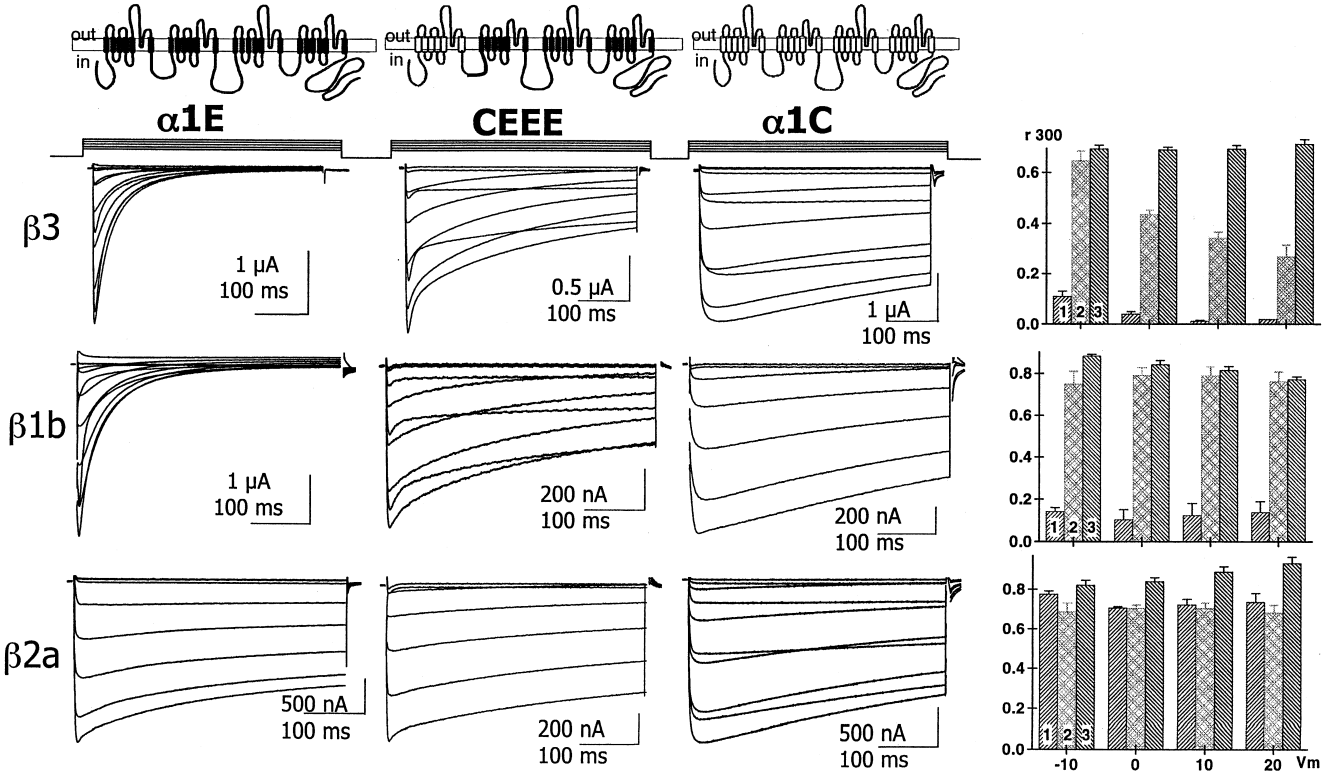


Fig. 2. (Left) $Ca_V2.3$, CEEE, and $Ca_V1.2$ were expressed with α2bδ and either β3, β1b, or β2a subunits in *Xenopus* oocytes. β3 induced the fastest and the most voltage-dependent inactivation kinetics. (Right) The fraction of the whole-cell currents remaining at the end of a 300-ms pulse (r300) was computed as a function of voltage with β3 (upper right), β1b (middle right), or β2a (lower right). In the presence of β3, r300 varied between 0.11 and 0.02 ($n=7$) for $Ca_V2.3$ (1) as compared to 0.67–0.25 ($n=5$) for CEEE (2) and 0.69–0.71 ($n=7$) for $Ca_V1.2$ (3). β2a yielded similar r300 values around 0.7–0.8 ($n=3$–8) for the three channels. Data were reported as mean ± S.E.M.

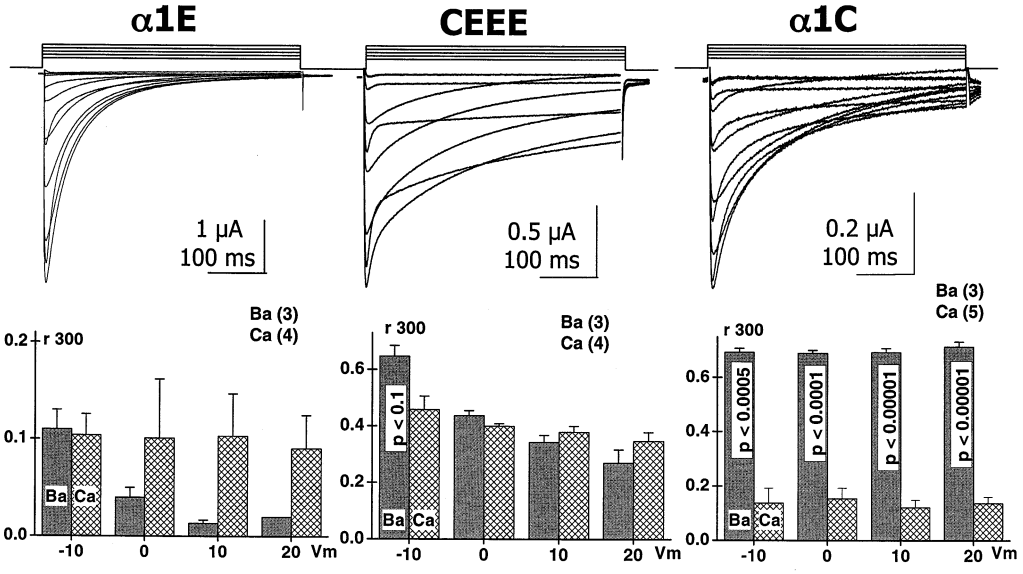


Fig. 3. Inactivation of CEEE was not modulated by $Ca^{2+}$. (Upper) $Ca_V2.3$ wt, CEEE, and $Ca_V1.2$ wt were co-expressed with α2bδ and β3 subunits in *Xenopus* oocytes and current traces measured in 10 mM $Ca^{2+}$. Voltage pulses (450 ms) were applied from −40 to +60 mV by 10-mV steps. (Lower) For CEEE, 41 ± 1% ($n = 4$) of the whole-cell $Ca^{2+}$ currents remained at the end of a 300-ms pulse to 0 mV which is not significantly different than the 44 ± 2% ($n = 3$) measured in the presence of $Ba^{2+}$. In contrast, r300 ratios for $Ca_V1.2$ were 0.69 ± 1 ($n = 3$) in $Ba^{2+}$ and 0.23 ± 1 ($n = 3$) in $Ca^{2+}$ solutions. Capacitive transients were erased for the first ms after the voltage step. Holding potential was −80 mV. Current scale varies between 0.1 and 1.0 μA. Time scales are 100 ms throughout.

$$I(t) = I_{\text{act}}\exp\left(-\frac{t-k}{\tau_{\text{act}}}\right) + I_{\text{1inact}}\exp\left(-\frac{t-k}{\tau_{\text{1inact}}}\right) + I_{\text{2inact}}\exp\left(-\frac{t-k}{\tau_{\text{2inact}}}\right) + C \quad (2)$$

Current traces were fitted to Eq. 2 where $I(t)$ is the current at time $t$; $\tau_{\text{act}}$; $\tau_{\text{1 inact}}$; $\tau_{\text{2 inact}}$ are respectively the activation, and the fast and slow inactivation time constants; $I_{\text{act}}$, $I_{\text{1 inact}}$, $I_{\text{2 inact}}$ indicate the relative amplitude of these processes; $k$ is the time at which the fit started; and $C$ is a fitting constant.

Inactivation kinetics were quantified using r300 values or the ratio of the whole-cell current remaining at the end of a 300 ms pulse [8]. Capacitive transients were erased for clarity in the final figures. Results are presented as mean ± S.E.M. Unpaired Students's *t*-test was used for statistical comparison.

## 3. Results

To address the role of Repeat I versus the I–II linker in the voltage-dependent inactivation of $Ca_V2.3$ channels, we have produced $Ca_V2.3$/$Ca_V1.2$ (EC) chimeric constructs. Fig. 1 shows the primary sequence alignment in the region encompassing the 5′ end of IS1 to the middle of the I–II linker. Within this region, 180 out of 340 residues are strictly conserved between $Ca_V1.2$ and $Ca_V2.3$. Hence, CEEE is more than 90% homologous to $Ca_V2.3$ while EC(*AID*)EEE differ from $Ca_V2.3$ by only 50 residues.

### 3.1. Part of Repeat I from $Ca_V1.2$ slows inactivation of $Ca_V2.3$ $Ca^{2+}$ channels

Whole-cell currents were recorded for $Ca_V2.3$, CEEE, and $Ca_V1.2$ expressed in *Xenopus* oocytes with α2bδ and either β3 (upper traces), β1b (middle traces), or β2a (lower traces) (Fig. 2). The swapping of Repeat I in CEEE significantly attenuated the inactivation kinetics as compared to $Ca_V2.3$ when expressed with either β3 or β1b. Co-injection with β2a blurred the difference in inactivation kinetics since β2a has been shown to decrease the voltage dependence of inactivation in $Ca_V2.3$ [22,27]. Current density did not appear to cause the slower inactivation kinetics of CEEE (Table 1).

The slower inactivation kinetics of CEEE were confirmed by the r300 ratio analysis (Fig. 2, right panel). The inactivation kinetics were modulated by β subunits in a similar fashion as the wild-type channels with β3 > β1b ≫ β2a [22]. CEEE tended to behave like $Ca_V1.2$ under any given condition. Nonetheless, the time course of CEEE inactivation retained a faster component which appears to be a distinctive feature of $Ca_V2.3$ inactivation kinetics. This faster time constant of inactivation, typically absent in $Ca_V1.2$ recordings, was observed with any β subunit tested. Despite significant changes in the inactivation kinetics, activation thresholds (results not shown) as well as activation kinetics were similar for CEEE and $Ca_V2.3$. Altogether, these results indicate that modifying Repeat I including part of the I–II linker, alters the inactivation kinetics of $Ca_V2.3$.

### 3.2. CEEE inactivation was not modulated by $Ca^{2+}$

Swapping Repeat I did not confer calcium-dependent inactivation onto $Ca_V2.3$ (Fig. 3). The inactivation kinetics of CEEE were not significantly different whether measured in $Ba^{2+}$, $Ca^{2+}$, or $Li^{+}$ (0 $Ca^{2+}$) (results not shown) thus ruling out a significant contribution from divalent-induced inactivation kinetics [28]. The current–voltage properties were similar for $Ca_V2.3$ and CEEE with peak voltages of $V_m = +6 \pm 1$ mV ($n = 3$) for $Ca_V2.3/\alpha2b\delta/\beta3$ and $V_m = +8 \pm 2$ mV ($n = 3$) for CEEE/α2bδ/β3 in contrast to $V_m = +14 \pm 2$ mV ($n = 3$) for the $Ca_V1.2/\alpha2b\delta/\beta3$. It should be noted that $Ca_V1.2$ peak currents were ≈5- to 6-fold smaller in $Ca^{2+}$ than in $Ba^{2+}$ whereas the current density of either CEEE or $Ca_V2.3$ was not significantly modulated by the nature of the charge carrier.

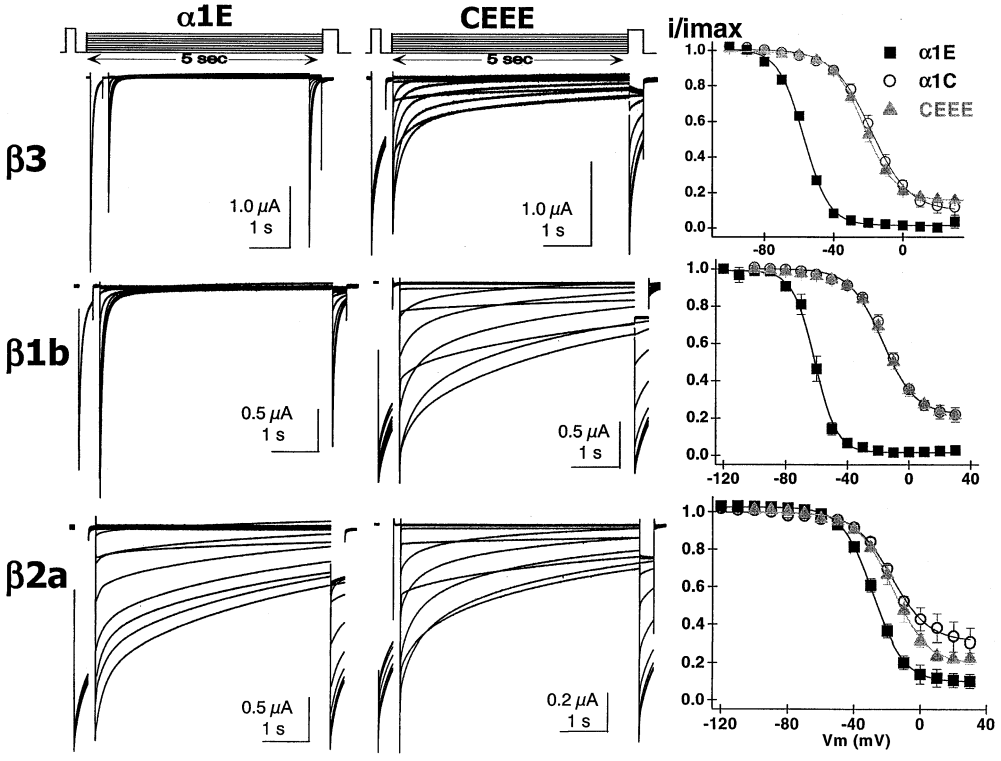


Fig. 4. $Ca_V2.3$, $Ca_V1.2$, and CEEE were co-expressed with α2bδ and either β3, β1b, or β2a in *Xenopus* oocytes. Isochronal inactivation was measured in $Ba^{2+}$ at a test pulse of 0 mV after a series of 5-s conditioning prepulses. The fraction of the non-inactivating current ($i/i_{max}$) is reported in the right panel. Smooth curves were generated using the fit parameters (Eq. 1). In the presence of β3, $z = 3.5 \pm 0.5$ and $E_{0.5} = -64 \pm 3$ mV for $Ca_V2.3$ ($n = 9$); $z = 2.7 \pm 0.3$ and $E_{0.5} = -23 \pm 1$ mV for CEEE ($n = 5$); $z = 3.2 \pm 0.2$ and $E_{0.5} = -23 \pm 1$ mV for $Ca_V1.2$ ($n = 8$). For β1b, $z = 3.5 \pm 0.4$ and $E_{0.5} = -61 \pm 1$ mV for $Ca_V2.3$ ($n = 5$); $z = 2.3 \pm 0.4$ and $E_{0.5} = -15 \pm 1$ mV for CEEE ($n = 6$); $z = 2 \pm 1$ and $E_{0.5} = -17 \pm 1$ mV for $Ca_V1.2$ ($n = 3$). For β2a, $z = 2.7 \pm 0.2$ and $E_{0.5} = -29 \pm 1$ mV for $Ca_V2.3$ ($n = 3$); $z = 2.3 \pm 0.7$ and $E_{0.5} = -18 \pm 1$ mV for CEEE ($n = 4$); $z = 2.3 \pm 0.7$ and $E_{0.5} = -17 \pm 1$ mV for $Ca_V1.2$ ($n = 3$). The fit values are shown with the estimated fit error.

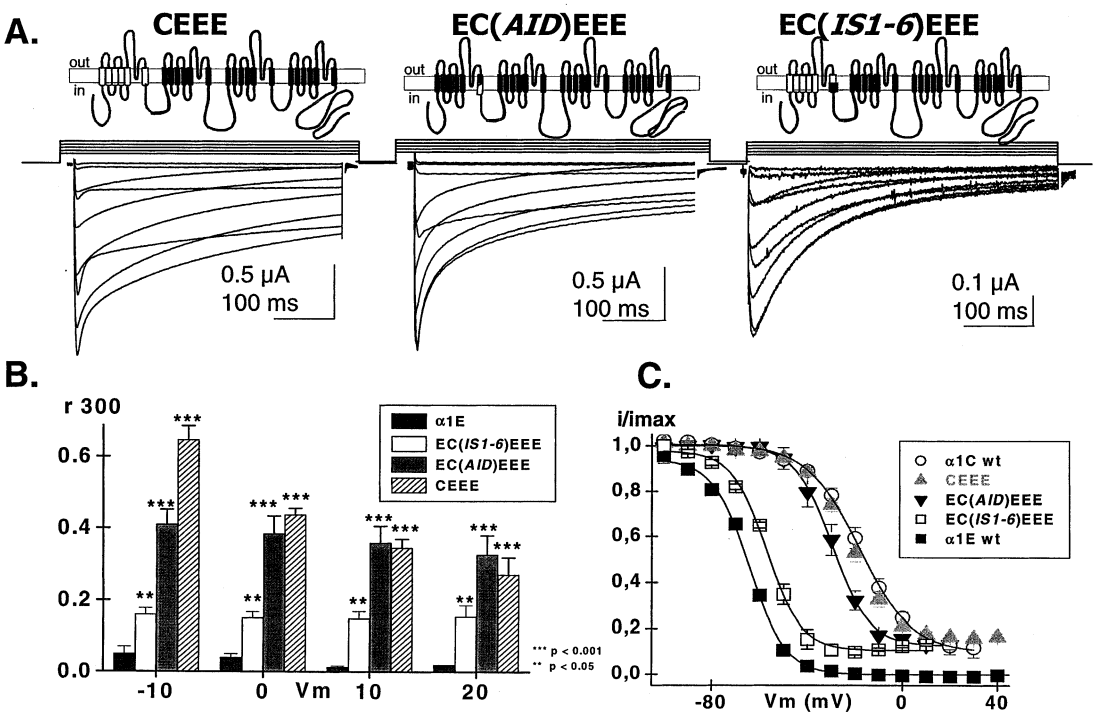


Fig. 5. (A) CEEE, EC(*AID*)EEE, and EC(*IS1–6*)EEE were expressed in *Xenopus* oocytes in the presence of α2bδ and β3 subunits. Whole-cell inactivation kinetics ranked (from the fastest to the slowest) $Ca_V2.3 > EC(IS1–6)EEE \gg EC(AID)EEE > CEEE$. (B) r300 ratio analysis. The r300 values ranged from $0.05 \pm 0.02$ to $0.02 \pm 0$ ($n = 10$) for $Ca_V2.3$; $0.16 \pm 0.02$ to $0.15 \pm 0.03$ ($n = 5$) for EC(*IS1–6*)EEE; $0.41 \pm 0.04$ to $0.32 \pm 0.05$ ($n = 6$) for EC(*AID*)EEE; and $0.65 \pm 0.04$ to $0.27 \pm 0.05$ ($n = 6$) for CEEE. Paired Student *t*-tests were performed with $^{**}P < 0.05$ and $^{***}P < 0.001$. (C) Isochronal inactivation data. EC(*IS1–6*)EEE and $Ca_V2.3$ inactivated in the same voltage range. Smooth curves were generated with Eq. 1 with $z = 3.5 \pm 0.4$ and $E_{0.5} = -57 \pm 1$ mV ($n = 4$) for EC(*IS1–6*)EEE, and $z = 3.2 \pm 0.3$ and $E_{0.5} = -30 \pm 1$ mV for EC(*AID*)EEE ($n = 6$). The fit values are shown with the estimated fit error.

More importantly, in contrast to the L-type $Ca_V1.2$ (α1C) channel, the inactivation of the chimera CEEE did not significantly speed up in the presence of 10 mM $Ca^{2+}$. Under these conditions, the fraction of whole-cell CEEE currents remaining at the end of a 300-ms pulse to 0 mV was $0.41 \pm 0.01$ ($n = 3$) which is similar to the $r300 = 0.44 \pm 0.02$ ($n = 3$) for $Ca_V1.2$ in 10 mM $Ba^{2+}$. The r300 ratios for $Ca_V2.3$ were also relatively similar with a value of $0.10 \pm 0.06$ ($n = 3$) in $Ca^{2+}$ and $0.04 \pm 0.02$ ($n = 3$) in $Ba^{2+}$. These data contrast with the r300 values for $Ca_V1.2$ that were significantly decreased ($P < 10^{-4}$) in the presence of $Ca^{2+}$ ($0.23 \pm 0.01$, $n = 3$) versus $Ba^{2+}$ ($0.69 \pm 0.01$, $n = 3$). These observations confirm that Repeat I in $Ca_V1.2$ does not confer calcium-dependent inactivation [3,8] and further suggest that the molecular determinants of calcium- and voltage-dependent inactivation are regulated by distinct sites on the calcium channel $Ca_V1.2$ subunit. Altogether, these results indicate that modifying Repeat I including part of the I–II linker, significantly decreases the voltage-dependent inactivation kinetics of $Ca_V2.3$.

### 3.3. Chimera CEEE inactivates in the same voltage range as $Ca_V1.2$

CEEE inactivated in the same voltage range as $Ca_V1.2$. The voltage dependence of CEEE inactivation was significantly shifted toward positive voltages as compared to $Ca_V2.3$ (Fig. 4). Isochronal inactivation was measured in $Ba^{2+}$ with either β3 (upper panel), β1b (middle panel), or β2a (lower panel). The fits to the Boltzmann equation are shown superimposed to the pooled data (Fig. 4, extreme right). As expected [22], the inactivation was typically

less voltage-dependent in the presence of β2a. Under any given condition, the inactivation of CEEE was significantly less voltage-dependent than $Ca_V2.3$.

### 3.4. Part of the I–II linker alters the inactivation kinetics of $Ca_V2.3$

The relative contribution of the I–II linker to the inactivation kinetics of CEEE was assessed using EC(*IS1–6*)EEE and EC(*AID*)EEE chimeras. EC(*AID*)EEE includes the region surrounding the β-subunit binding site from $Ca_V1.2$ (Fig. 1). Typical $Ba^{2+}$ current traces are shown (Fig. 5A). The whole-cell *I–V* properties were similar for the 3 chimeras with peak voltages of $0 \pm 1$ mV ($n=3$) for CEEE, $-3 \pm 3$ mV ($n=4$) for EC(*AID*)EEE, $4 \pm 3$ mV ($n=4$) for EC(*IS1–6*)EEE, and $-2 \pm 3$ mV ($n=3$) for $Ca_V2.3$. In the presence of β3, inactivation kinetics ranked $Ca_V2.3 >$ EC(*IS1–6*)EEE $\gg$ EC(*AID*)EEE $>$ CEEE (from the fastest to the slowest).

The r300 analysis (Fig. 5B) confirms that the inactivation kinetics of CEEE and EC(*AID*)EEE were comparable. EC(*AID*)EEE was slightly faster than CEEE at −10 mV ($P<0.2$) but remained nonetheless significantly slower than $Ca_V2.3$ and EC(*IS1–6*)EEE ($P<0.001$). EC(*IS1–6*)EEE chimera behaved mostly like $Ca_V2.3$ although its inactivation kinetics remained reproducibly a little slower than $Ca_V2.3$ ($P<0.05$). Hence, the AID motif appears to exert the strongest effect on inactivation kinetics of $Ca_V2.3$ although the transmembrane segments in Repeat I are not completely devoid of influence.

The voltage dependence of inactivation for EC(*AID*)EEE was shifted toward more positive potentials as compared to $Ca_V2.3$ although it remained slightly more negative than CEEE and $Ca_V1.2$ inactivation (Fig. 5C). Even though EC(*1S1–6*)EEE and $Ca_V2.3$ inactivated in the same voltage range, a significant fraction ($\approx 10\%$) of the whole-cell currents from EC(*1S1–6*)EEE failed to inactivate after a 5 s pulse to 0 mV.

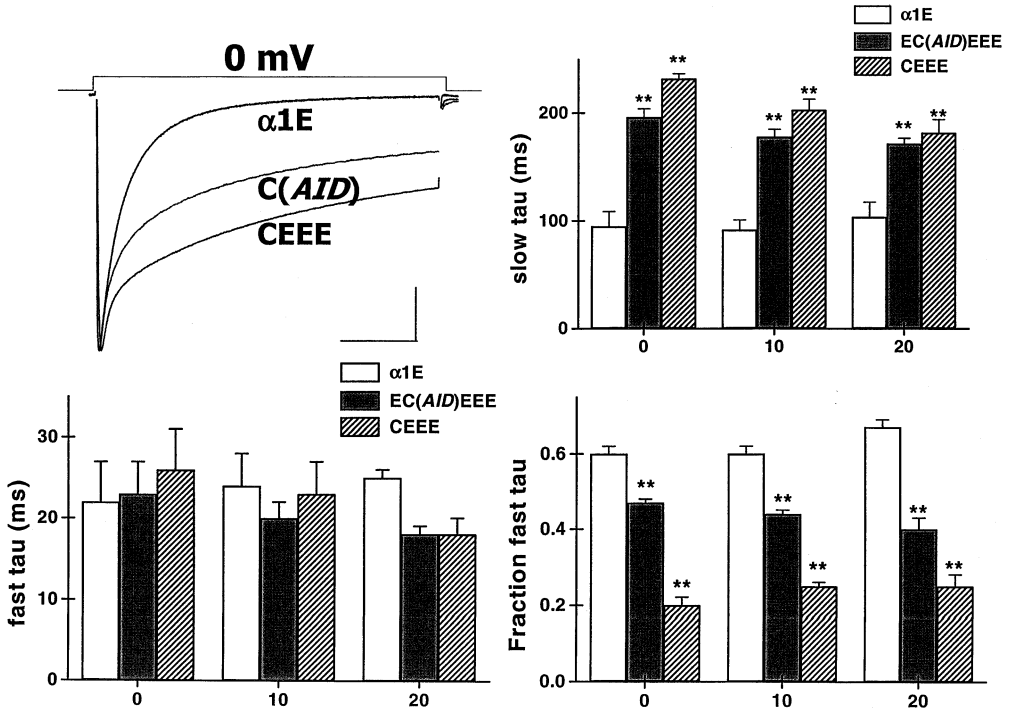


Fig. 6. (Upper left) Whole-cell $Ba^{2+}$ currents obtained at 0 mV for $Ca_V2.3$, CEEE, and EC(*AID*)EEE were scaled and superimposed. (Upper right) Currents were fitted to Eq. 2. The slow inactivation $\tau$ became increasingly slower from $Ca_V2.3$ to CEEE going from $96 \pm 14$ ms ($n=3$) for $Ca_V2.3$ to $232 \pm 5$ ms ($n=3$) for CEEE at 0 mV. (Lower left) The fast inactivation $\tau$ remained stable with values of $22 \pm 5$ ms ($n=3$) for $Ca_V2.3$, $23 \pm 4$ ms ($n=3$) for EC(*AID*)EEE, and $31 \pm 5$ ms ($n=3$) for CEEE at 0 mV. (Lower right) The relative contribution of $\tau_{fast}$ decreased from $Ca_V2.3$ to CEEE with $0.6 \pm 0.2$ ($n=3$) for $Ca_V2.3$, $0.47 \pm 0.01$ ($n=3$) for EC(*AID*)EEE, and $0.18 \pm 0.03$ for CEEE at 0 mV. Paired Student *t*-test was performed with $^{**}P<0.01$. Scales are 0.2 and 100 ms.

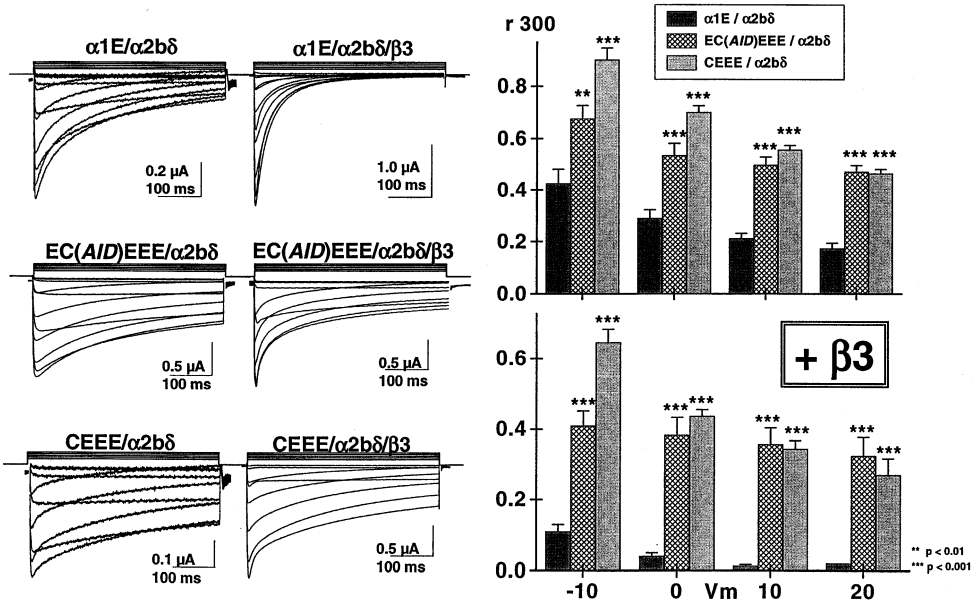


Fig. 7. β3 subunit modulation. (Left) CEEE, EC(*AID*)EEE, and $Ca_V2.3$ were expressed with α2bδ (extreme left) or α2bδ/β3 subunits (left). β3 sped up inactivation kinetics of either CEEE, EC(*AID*)EEE, or $Ca_V2.3$. (Right) This observation is confirmed by the r300 values. At −10 mV, r300 went from 0.53 ± 0.05 (α2bδ) to 0.11 ± 0.02 (α2bδ/β3) ($n = 3$) for $Ca_V2.3$; from 0.90 ± 0.05 (α2bδ) to 0.65 ± 0.08 (α2bδ/β3) ($n = 3$) for CEEE; and from 0.68 ± 0.09 (α2bδ) to 0.41 ± 0.04 (α2bδ/β3) ($n = 5$) for EC(*AID*)EEEE. R300 values for EC(*AID*)EEE and CEEE significantly differed ($P < 0.001$) from $Ca_V2.3$ when measured upon the same background. Paired Student *t*-test was performed using experiments pooled from three independent series of injections with $^{**}P < 0.01$ and $^{***}P < 0.001$.

### 3.5. The I–II linker decreased the slow (100–200 ms) inactivation τ in $Ca_V2.3$

Within our experimental conditions, the inactivation kinetics of $Ca_V2.3$ could be easily described by a sum of two exponential functions with the fast inactivation time constant (≈20–30 ms) being predominant. As already observed earlier, a non-negligible fraction of CEEE and EC(*AID*)EEE currents retained this trademark fast (≈20–30 ms) inactivation process (Figs. 2 and 5A). A detailed kinetic analysis revealed that this fast inactivation time constant ($\tau_{1\ inact}$ or $\tau_{fast}$) remained remarkably constant while the contribution of $\tau_{fast}$ progressively decreased from the wild-type channel $Ca_V2.3$ (≈0.65) to EC(*AID*)-EEE (≈0.45) to CEEE (≈0.25) (Fig. 6). Conversely, the introduction of $Ca_V1.2$ fragments into $Ca_V2.3$ appeared to increase the slow inactivation time constant ($\tau_{2\ inact}$ or $\tau_{slow}$) from ≈90 to 105 ms in $Ca_V2.3$ to ≈190 to 235 ms in CEEE. The persistence of this fast inactivation time constant in the both chimeras recordings suggests a small but non-negligible contribution from other regions of $Ca_V2.3$ to the inactivation process.

### 3.6. Inactivation kinetics in the absence of exogenous β subunits

The AID region plays a critical role in modulating $Ca^{2+}$ channel function. β subunits are chaperoning the α1 subunit to the plasma membrane [29–31] and are speeding up inactivation kinetics [22,32] by presumably binding to the AID motif located in the I–II linker [33,34]. To evaluate whether β-subunit modulation of inactivation was preserved in our chimeras, oocytes were injected under paired conditions with the same endogenous β-subunit background, in the presence (α2bδ/β3) and in the absence of exogenous β3 (with α2bδ).

Typical current traces recorded in $Ba^{2+}$ are shown in Fig. 7. β3 sped up inactivation kinetics as confirmed by the r300 analysis (Fig. 7, right panels). Under all conditions, whole-cell currents were typically 50- to 100-fold larger than the endogenous $Ca^{2+}$ currents in oocytes [29]. Peak current expression was increased in the presence of β3 going from −0.63 ± 0.03 μA ($n = 3$) to −2.7 ± 0.3 μA ($n = 3$) for $Ca_V2.3$; from −1.2 ± 0.3 μA ($n = 3$) to −1.8 ± 0.3 μA ($n = 3$) for EC(*AID*)EEE; from −0.41 ± 0.01 μA

($n=3$) to $-1.4\pm0.5$ μA ($n=3$) for CEEE; from $-0.86\pm0.06$ μA ($n=3$) to $-2.5\pm0.4$ μA ($n=3$) for $Ca_V1.2$. Co-injection with β3 induced a typical leftward shift of the peak voltage by −10 mV (results not shown) [22]. Hence, CEEE and EC(*AID*)EEE chimeras displayed the typical hallmarks of β-subunit modulation in $Ca^{2+}$ channels. More importantly, inactivation kinetics ranked EC(*AID*)EEE ≈ CEEE ≪ $Ca_V2.3$ (from the slowest to the fastest) whether they were measured in the absence (Fig. 7, upper right panel) or in the presence of exogenous β3 (Fig. 7, lower right panel). Hence, CEEE and EC(*AID*)EEE remained distinctively different from $Ca_V2.3$ in the absence of exogenous β3.

## 4. Discussion

### 4.1. The role of Repeat I and the I–II linker in the inactivation kinetics of $Ca_V2.3$

Voltage-dependent inactivation of $Ca_V2.3$ (α1E) channels was investigated at the molecular level using chimeric constructs between two high-voltage activated $Ca^{2+}$ channels $Ca_V2.3$ and $Ca_V1.2$. These two channels inactivate through different mechanisms. $Ca_V2.3$ undergoes fast and mostly voltage-dependent inactivation [35–37] whereas $Ca_V1.2$ experiences very little voltage-dependent inactivation under most experimental conditions. It is now widely believed that $Ca_V1.2$ inactivates under physiological conditions mostly through a calcium/calmodulin dependent mechanism which could explain its relatively slow kinetics in the complete absence of $Ca^{2+}$ [22].

Our study focused on CEEE and EC(*AID*)EEE chimeras to investigate the contribution of Repeat I and the cytoplasmic region surrounding the β-subunit binding site to the voltage-dependent inactivation of $Ca_V2.3$ [14,15]. The inactivation kinetics were significantly slowed when Repeat I of $Ca_V2.3$ was swapped with the same region of $Ca_V1.2$ in the CEEE chimera. The chimera CEEE with Repeat I from $Ca_V1.2$ and EC(*AID*)EEE, containing AID from $Ca_V1.2$, were co-expressed in *Xenopus* oocytes with α2bδ and either β3, β1b, or β2a subunits. CEEE and EC(*AID*)EEE chimera were modulated by β subunits which ranked β3 > β1b > β2a with respect to inactivation kinetics and voltage dependence just like the wild-type $Ca_V2.3$ and $Ca_V1.2$ channels [22]. Under most experimental conditions tested, both chimeras significantly differed from $Ca_V2.3$. In the presence of 10 mM $Ba^{2+}$, the r300 values for EC(*AID*)EEE and CEEE were respectively ≈0.4 and ≈0.65 which are significantly different ($P<10^{-3}$) from the r300 of ≈0.1 for the wild-type $Ca_V2.3$. The voltage dependence of inactivation was also significantly shifted toward $Ca_V1.2$ with mid-points of inactivation ($E_{0.5}$) set at $-23\pm2$ mV for CEEE and $-30\pm2$ mV for EC(*AID*)EEE as compared to $-64\pm3$ mV for $Ca_V2.3$ and $-23\pm3$ mV for $Ca_V1.2$. Hence, the change in the inactivation properties appears to be related to the importance of the $Ca_V1.2$ fragment introduced into the channel host.

Whereas the inactivation kinetics measured the time course of the channel transitions from the open to the inactivated state, the isochronal inactivation data characterized the voltage range where transitions to the inactivated state occur. It has been suggested that $Ca_V2.3$ channels could inactivate partially from the closed state which is not contradicted by the mid-point of inactivation of −64 mV featured in our study [38]. In contrast, the isochronal inactivation data of $Ca_V1.2$, CEEE, and EC(*AID*)EEE clearly overlapped with their respective activation properties suggesting that they could inactivate mostly from the open state. Hence, the changes in the voltage dependence of inactivation observed in the chimeras seemed to indicate that AID from $Ca_V1.2$ contains critical elements that prevent inactivation from negative membrane potentials. As AID contains the high-affinity binding site for β subunits, we examined the possibility that the slower inactivation kinetics were caused by a decreased modulation by the β subunit. Our results showed that the rates of inactivation for $Ca_V2.3 \gg$ EC(*AID*)EEE ≫ CEEE were independent of the exogenous β3. These observations were not surprising considering that the AID motif does not constitute the unique interaction site between β subunits and $Ca_V2.3$ [29] and that β-subunit modulation of $Ca_V1.2$ channels could be achieved without normal β binding to the AID motif [30,31]. Although our experiments could not completely rule out subtle alterations in the endogenous β-subunit modulation, such modifications are unlikely to account for our data. Endogenous oocyte β subunits (β3xo) are apparently unable to modulate

significantly the gating properties of $Ca_V2.3$ channels [29].

Furthermore, all other properties such as peak expression up-regulation, negative shift in the peak current–voltage relationships as well as the negative shift in the steady-state inactivation curve were maintained. Altogether, our data suggest a critical functional role for the cytoplasmic region surrounding AID in $Ca_V2.3$ inactivation.

The role of the cytoplasmic fragment surrounding the β-subunit binding motif (AID) in the I–II linker was underscored by the distinct inactivation properties of EC(*IS1–6*)EEE and EC(*AID*)EEE chimeras. As EC(*AID*)EEE and $Ca_V2.3$ are identical but for 50 residues in the I–II linker, our data suggest that this region is critical to ensure fast inactivation kinetics in $Ca_V2.3$ channels. At this point, the systematic lack of expression in oocytes from the reverse chimeras ECCC and CE(*AID*)CCC prevents us from concurring about the role of this region in $Ca_V1.2$ inactivation kinetics.

Although the region surrounding the AID motif is critical, it is clearly not the unique determinant of inactivation in $Ca_V2.3$. EC(*AID*)EEE remained reproducibly faster than CEEE which inactivated at faster rate than $Ca_V1.2$. Furthermore, substitution of the AID region by its $Ca_V1.2$ equivalent appeared to decrease but not completely eliminate fast inactivation kinetics, indicating that the inactivation gating of $Ca_V2.3$ was not fully accounted for by the I–II linker or the Repeat I. Indeed the kinetic analysis of the chimera recordings revealed the persistence of the fast inactivation time constant, suggesting a non-negligible contribution from other regions of $Ca_V2.3$. Furthermore, some voltage-dependent inactivation remained in the CEEE chimera, suggesting that repeat I plus the AID region could not account completely for the voltage dependence of inactivation. Finally, the EC(*IS1–6*)EEE chimera displayed inactivation kinetics slightly slower than $Ca_V2.3$.

### 4.2. Molecular determinants of inactivation within the AID motif

In addition to our own data, recent studies have strongly suggested a critical role for the I–II linker in the inactivation of voltage-dependent $Ca^{2+}$ channels (VDCC) [17,39–42]. As the AID motif is conserved in all non T-type α1 subunits, this observation suggests a role for nonconserved residues present in the AID domain. The AID binding site is composed of 18 residues (**QQXEXXLXGYXXWIXXXE)** and is strictly conserved in non-T-type $Ca_V1$ and $Ca_V2$ families. We have recently analyzed the role of the nonconserved residues within that motif [18]. The quintuple mutant $Ca_V2.3$ N381K+R384L+A385D+D388T+K389Q (NRADK-KLDTQ) inactivated like the wild-type channels. In contrast, point mutations of R378 in $Ca_V2.3$ (position 5 of AID) into negatively charged residues Glu (E) or Asp (D) significantly slowed inactivation kinetics and shifted the voltage dependence of inactivation to more positive voltages. The reverse mutation E462R in $Ca_V1.2$ produced channels with inactivation properties comparable to $Ca_V2.3$ R378E suggesting that the charge of the nonconserved residue at position 5 of the AID motif in the I–II linker could significantly alter the inactivation of $Ca_V1.2$ and $Ca_V2.3$ channels. Despite these significant changes, none of these mutations could completely eliminate voltage- dependent inactivation in $Ca_V2.3$ [18].

### 4.3. Comparison with other studies

Mutagenesis studies of voltage-dependent in $Ca^{2+}$ channels has shed some light regarding the molecular mechanism of inactivation. In the landmark study by the group of Tsien, voltage-dependent inactivation was investigated by inserting $Ca_V2.1$ (α1A) fragments into the $Ca_V2.3$ channel [14]. Their conclusion supported a critical role for IS6 in the voltage-dependent inactivation of $Ca_V2.1$ and $Ca_V2.3$ channels [14]. A careful look into their observations however suggests some similarities to our own data. Their DB9 chimera with the Repeat I+part of the I–II linker from the slow $Ca_V2.1$ conferred slow inactivation kinetics to the host $Ca_V2.3$ in a manner similar to our CEEE chimera. Their shorter chimera DB19, in which a 140 aa fragment from $Ca_V2.1$ was inserted into $Ca_V2.3$, was larger by 50 aa than our EC(*AID*)EEE but stretched over a similar region from the 5′ end of IS6 to 52 aa beyond the 3′ end of the AID motif. Like EC(*AID*)EEE, the DB19 chimera, displayed slow inactivation kinetics similar to $Ca_V2.1$ and seemingly distinct from $Ca_V2.3$. Likewise, their DB10 chimera, similar to our EC(*IS1–6*)EEE, dis-

played the typical inactivation phenotype of $Ca_V2.3$ channels. One of the major difference could reside in the observation that inserting IS6 from $Ca_V2.3$ in the DB18 chimera, between the 3′ end of Pore I up to 5′ end of the AID motif could significantly accelerate the inactivation kinetics of $Ca_V2.1$. However, both sets of data are not completely incompatible since the two most critical residues in the DB18 chimera were identified in the region stretching between the middle of IS6 and the AID motif.

The focus has shifted, over recent years, from the transmembrane regions toward the cytoplasmic linkers. Overexpression of mRNA coding for the I–II linker from $Ca_V2.1$, but not for the III–IV linker, was shown to speed up inactivation of wild-type $Ca_V2.1/\beta2a$ in *Xenopus* oocytes [42]. Point mutations and/or chimeras in that region modified inactivation kinetics in $Ca_V2.1$ [40,43], $Ca_V2.3$ [18,39], and $Ca_V1.2$ channels [18,40,41]. It is significant to note that a single valine insertion in the I–II linker dramatically slowed the inactivation kinetics of a $Ca_V2.1$ splice variant [43]. This natural mutation occurs in the same region covered in our EC(*AID*)EEE chimera. Furthermore, insertion of the I–II linker region from $Ca_V2.3$ was shown to accelerate the inactivation kinetics of $Ca_V1.2$ and caused a $-20$ mV shift in its half-potential of inactivation [17]. This result agrees with our EC(*AID*)EEE data since inserting part of the I–II linker from $Ca_V1.2$, which caused a significant decrease into the inactivation kinetics of $Ca_V2.3$. Finally, we have recently shown that nonconserved residues within the AID motif of $Ca_V1.2$ and $Ca_V2.3$ significantly altered voltage-dependent inactivation properties in both channels [18]. Hence mutations in the 5′ end of the I–II linker appeared to modify extensively the inactivation properties of $Ca_V1$ and $Ca_V2$ calcium channel families. It remains to be seen whether this molecular determinant plays a critical role in $Ca_V3$ T-type $Ca^{2+}$ channels which lack the consensus AID motif in the I–II linker.

By analogy with $K^+$ and $Na^+$ channels, we could speculate that the I–II linker of $Ca_V2.3$ could contribute to voltage-dependent inactivation by either forming a inactivating blocking particle or contributing to C-type inactivation [44,45]. β subunits could be envisioned to regulate $Ca^{2+}$ channel inactivation kinetics by priming the I–II linker into a conformation more favorable to inactivation. Possible determinants for the receptor of the inactivating particle could include the C-terminus which has been shown to modulate calcium- [2,4–6,46] and voltage-dependent [3,47] inactivation.

## Acknowledgements

We thank Dr. Ed Perez-Reyes for the rabbit $Ca_V1.2$, β2a, β1b, and β3 subunits; Dr. Toni Schneider for the human $Ca_V2.3$; and Dr. R. Sauvé for critical reading. L.P. is a Senior scholar from the 'Fonds de la Recherche en Santé du Québec'. This work was completed with grants from the Medical Research Council of Canada MT13390 and the Canadian Heart and Stroke Foundation to L.P.

## References

[1] W.A. Catterall, Annu. Rev. Cell Dev. Biol. 16 (2000) 521–555.
[2] M. deLeon, Y. Wang, L. Jones, E. Perez-Reyes, X. Wei, T.W. Soong, T.P. Snutch, D.T. Yue, Science 270 (1995) 1502–1506.
[3] G. Bernatchez, D. Talwar, L. Parent, Biophys. J. 75 (1998) 1727–1739.
[4] N. Qin, R. Olcese, M. Bransby, T. Lin, L. Birnbaumer, Proc. Natl. Acad. Sci. USA 96 (1999) 2435–2438.
[5] R.D. Zuhlke, G.S. Pitt, K. Deisseroth, R.W. Tsien, H. Reuter, Nature 399 (1999) 159–162.
[6] B.Z. Peterson, C.D. DeMaria, J.P. Adelman, D.T. Yue, Neuron 22 (1999) 549–558.
[7] A. Lee, S.T. Wong, D. Gallagher, B. Li, D.R. Storm, T. Scheuer, W.A. Catterall, Nature 399 (1999) 155–159.
[8] B.Z. Peterson, J.S. Lee, J.G. Mulle, Y. Wang, L.M. de, D.T. Yue, Biophys. J. 78 (2000) 1906–1920.
[9] T. Hoshi, W.N. Zagotta, R.W. Aldrich, Science 250 (1990) 533–538.
[10] S. Kellenberger, T. Scheuer, W.A. Catterall, J. Biol. Chem. 271 (1996) 30971–30979.
[11] C.A. Rohl, F.A. Boeckman, C. Baker, T. Scheuer, W.A. Catterall, R.E. Klevit, Biochemistry 38 (1999) 855–861.
[12] T. Tanabe, B.A. Adams, S. Numa, K.G. Beam, Nature 352 (1991) 800–803.
[13] J. Nakai, B.A. Adams, K. Imoto, K.G. Beam, Proc. Natl. Acad. Sci. USA 91 (1994) 1014–1018.
[14] J.F. Zhang, P.T. Ellinor, R.W. Aldrich, R.W. Tsien, Nature 372 (1994) 97–100.

[15] L. Parent, M. Gopalakrishnan, A.E. Lacerda, X. Wei, E. Perez-Reyes, FEBS Lett. 360 (1995) 144–150.
[16] R.L. Spaetgens, G.W. Zamponi, J. Biol. Chem. 274 (1999) 22428–22436.
[17] S.C. Stotz, J. Hamid, R.L. Spaetgens, S.E. Jarvis, G.W. Zamponi, J. Biol. Chem. 275 (2000) 24575–24582.
[18] L. Berrou, G. Bernatchez, L. Parent, Biophys. J. 80 (2001) 215–228.
[19] L. Parent, G. Bernatchez, L. Berrou, Z. Benakezouh, J. Ducay, Biophys. J. 80 (2001) 620a.
[20] J. Sambrook, E.F. Fritsch, T. Maniatis, Molecular Cloning: A Laboratory Manual, 2nd Edition, Cold Spring Harbor Laboratory, Cold Spring Harbor, NY, 1989.
[21] L. Parent, M. Gopalakrishnan, Biophys. J. 69 (1995) 1801–1813.
[22] L. Parent, T. Schneider, C.P. Moore, D. Talwar, J. Membr. Biol. 160 (1997) 127–140.
[23] M.E. Williams, D.H. Feldman, A.F. McCue, R. Brenner, G. Velicelebi, S.B. Ellis, M.M. Harpold, Neuron 8 (1992) 71–84.
[24] A. Castellano, X. Wei, L. Birnbaumer, E. Perez-Reyes, J. Biol. Chem. 268 (1993) 3450–3455.
[25] E. Perez-Reyes, A. Castellano, H.S. Kim, P. Bertrand, E. Baggstrom, A.E. Lacerda, X.Y. Wei, L. Birnbaumer, J. Biol. Chem. 267 (1992) 1792–1797.
[26] M. Pragnell, J. Sakamoto, S.D. Jay, K.P. Campbell, FEBS Lett. 291 (1991) 253–258.
[27] R. Olcese, N. Qin, T. Schneider, A. Neely, X. Wei, E. Stefani, L. Birnbaumer, Neuron 13 (1994) 1433–1438.
[28] G. Ferreira, J. Yi, E. Rios, R. Shirokov, J. Gen. Physiol. 109 (1997) 449–461.
[29] E. Tareilus, M. Roux, N. Qin, R. Olcese, J. Zhou, E. Stefani, L. Birnbaumer, Proc. Natl. Acad. Sci. USA 94 (1997) 1703–1708.
[30] H. Yamaguchi, M. Hara, M. Strobeck, K. Fukasawa, A. Schwartz, G. Varadi, J. Biol. Chem. 273 (1998) 19348–19356.
[31] U. Gerster, B. Neuhuber, K. Groschner, J. Striessnig, B.E. Flucher, J. Physiol. (Lond.) 517 (Pt 2) (1999) 353–368.
[32] L.L. Isom, K.S. DeJongh, W.A. Catterall, Neuron 12 (1994) 1183–1194.
[33] M. Pragnell, M. De Waard, Y. Mori, T. Tanabe, T.P. Snutch, K.P. Campbell, Nature 368 (1994) 67–70.
[34] A. Hohaus, M. Poteser, C. Romanin, N. Klugbauer, F. Hofmann, I. Morano, H. Haase, K. Groschner, Biochem. J. 348 (2000) 657–665.
[35] P.T. Ellinor, J.F. Zhang, A.D. Randall, M. Zhou, T.L. Schwarz, R.W. Tsien, W.A. Horne, Nature 363 (1993) 455–458.
[36] M. Wakamori, T. Niidome, D. Furutama, T. Furuichi, K. Mikoshiba, Y. Fujita, I. Tanaka, K. Katayama, A. Yatani, A. Schwartz, Receptors Channels 2 (1994) 303–314.
[37] T. Schneider, X. Wei, R. Olcese, J.L. Costantin, A. Neely, P. Palade, E. Perez-Reyes, N. Qin, J. Zhou, G.D. Crawford, R.G. Smith, S.H. Appel, E. Stefani, L. Birnbaumer, Receptors Channels 2 (1994) 255–270.
[38] P.G. Patil, D.L. Brody, D.T. Yue, Neuron 20 (1998) 1027–1038.
[39] K.M. Page, G.J. Stephens, N.S. Berrow, A.C. Dolphin, J. Neurosci. 17 (1997) 1330–1338.
[40] S. Herlitze, G.H. Hockerman, T. Scheuer, W.A. Catterall, Proc. Natl. Acad. Sci. USA 94 (1997) 1512–1516.
[41] B. Adams, T. Tanabe, J. Gen. Physiol. 110 (1997) 379–389.
[42] T. Cens, S. Restituito, S. Galas, P. Charnet, J. Biol. Chem. 274 (1999) 5483–5490.
[43] E. Bourinet, T.W. Soong, K. Sutton, S. Slaymaker, E. Mathews, A. Monteil, G.W. Zamponi, J. Nargeot, T.P. Snutch, Nat. Neurosci. 2 (1999) 407–415.
[44] A.M. VanDongen, G.C. Frech, J.A. Drewe, R.H. Joho, A.M. Brown, Neuron 5 (1990) 433–443.
[45] T. Hoshi, W.N. Zagotta, R.W. Aldrich, Neuron 7 (1991) 547–556.
[46] J. Zhou, R. Olcese, N. Qin, F. Noceti, L. Birnbaumer, E. Stefani, Proc. Natl. Acad. Sci. USA 94 (1997) 2301–2305.
[47] U. Klockner, G. Mikala, M. Varadi, G. Varadi, A. Schwartz, J. Biol. Chem. 270 (1995) 17306–17310.